Case Studies in Thermal Engineering 61 (2024) 104798

Contents lists available at ScienceDirect

Case Studies in Thermal Engineering

journal homepage: www.elsevier.com/locate/csite

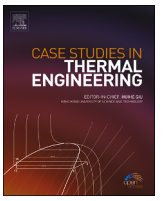

Numerical exploration of the impact of fluid type in a uniquely designed shell and spiral tube heat exchanger

Naim Ben Ali [a], Dheyaa Jumaah Jasim [b], Saman Aminian [c], Pradeep Kumar Singh [d], Husam Rajab [e], Ismail M.M.Elsemary [f, g], Lioua Kolsi [h], Neaman Sohrabi [i], Reza Haddadvand [i], Seyyed Amirreza Abdollahi [j, *]

[a] Department of Industrial Engineering, College of Engineering, University of Ha'il, Ha'il City 81451, Saudi Arabia
[b] Department of Petroleum Engineering, Al-Amarah University College, Maysan, Iraq
[c] Department of Civil Engineering, College of Engineering, Cihan University-Erbil, Erbil, Iraq
[d] Department of Mechanical Engineering, Institute of Engineering and Technology, GLA University, Mathura, U.P., India
[e] College of Engineering, Mechanical Engineering Department, Alasala University, King Fahad Bin Abdulaziz Rd., P.O.Box: 12666, Amanah: 31483, Dammam, Kingdom of Saudi Arabia
[f] Department of Mechanical Engineering, College of Engineering, Northern Border University, Arar, 91431, Saudi Arabia
[g] Combustion and Energy Technology Lab, Mechanical Engineering Department, Shoubra Faculty of Engineering, Benha University, 108 Shoubra Street, Cairo, Egypt
[h] Department of Mechanical Engineering, College of Engineering, University of Ha'il, Ha'il City, Saudi Arabia
[i] Department of Mechanical and Mechatronics Engineering, Southern Illinois University, Edwardsville, IL, USA
[j] Faculty of Mechanical Engineering, University of Tabriz, Tabriz, Iran

ARTICLE INFO

Handling Editor: Huihe Qiu

Keywords:
Thermohydraulic performance
Shell-and-coil tube heat exchanger
Friction coefficient
Hybrid nanofluid

ABSTRACT

Shell and spiral tube heat exchangers are widely favored in refrigeration and applications such as heat recovery systems, food processing, and heat storage. Researchers' primary focus is to discover a simple and cost-effective approach to improve the efficiency of heat exchangers. The research employed a specially designed shell and spiral tube heat exchanger to enhance efficiency. This research involved utilizing ANSYS FLUENT CFD software to analyze the thermodynamic efficiency and predict heat transfer in the specified converter. The analysis incorporated factors such as displacement velocity coefficient and friction coefficient. Researchers are focused on finding a simple and cost-effective approach to improve the efficiency of heat exchangers. Furthermore, the selection of nanohybrid fluids is a crucial factor influencing the thermohydraulic performance of shell and spiral tube heat exchangers. Among the three fluid nanohybrids chosen for simulation, the water nanohybrid exhibited superior temperature performance, surpassing all other liquids. Furthermore, the optimal thermal performance for the hybrid nanofluid was observed at $\varphi_1 = \varphi_2 = 0.7$.

1. Introduction

Many people mistake the spiral heat exchanger for a modern invention. However, a spiral pattern was first proposed in the 19th century. The delay in progressing to a complete product until the 1930s was caused solely by an absence of suitable materials and manufacturing methods. The utilization of spiral heat exchangers has been on the rise, with their application expanding across sectors

* Corresponding author.
E-mail address: s.a_abdollahi@yahoo.com (S.A. Abdollahi).

https://doi.org/10.1016/j.csite.2024.104798
Received 17 April 2024; Received in revised form 27 June 2024; Accepted 5 July 2024
Available online 10 July 2024

Table 1
Specifics relating to the shell and tube, which are helically twisted [27].

Parameter	Value
Interior diameter of coiled tube	**0.007**
Exterior diameter of coiled tube	**0.008**
Coil diameter	**0.1**
Coil pitch	**0.017**
Number of turns	**18**
Shell diameter	**0.15**
Shell height	**0.377**
Inner tube diameter	**0.060**
Inner tube height	**0.335**

like chemicals, steel, pulp, and paper. S. Kim et al. [1] researched shell coil and helically shaped tube heat exchangers, exploring different dimple configurations across various Dean numbers and input temperature rangesThe pressure drop, Nusselt number, and temperature difference were computed using three-dimensional Reynolds-Averaged Navier-Stokes (RANS) equations. An optimal node count of approximately 190 million was determined through grid dependency analysis. The numerical findings aligned closely with experimental data, showing that inline and staggered configurations exhibited the highest temperature differences and lowest pressure reductions. A study by A. Alimoradi et al. explored the application of annular fins to enhance heat transfer between the shell and the helical coil heat exchanger. Thirteen heat exchangers were designed and tested across three different shell-side Reynolds numbers. Two approaches were employed to validate the numerical model: comparing heat transfer coefficients on the shell sides through approximation methods and conducting thermal transfer calculations. The results showed that heat transfer rates can increase by up to 44.11 % within the range of 7500–30000 [2]. This study addresses the critical question of efficiently removing heat from surfaces with high-temperature flux using tabulators and components with specific geometries [3]. This study's critical hypothesis revolves

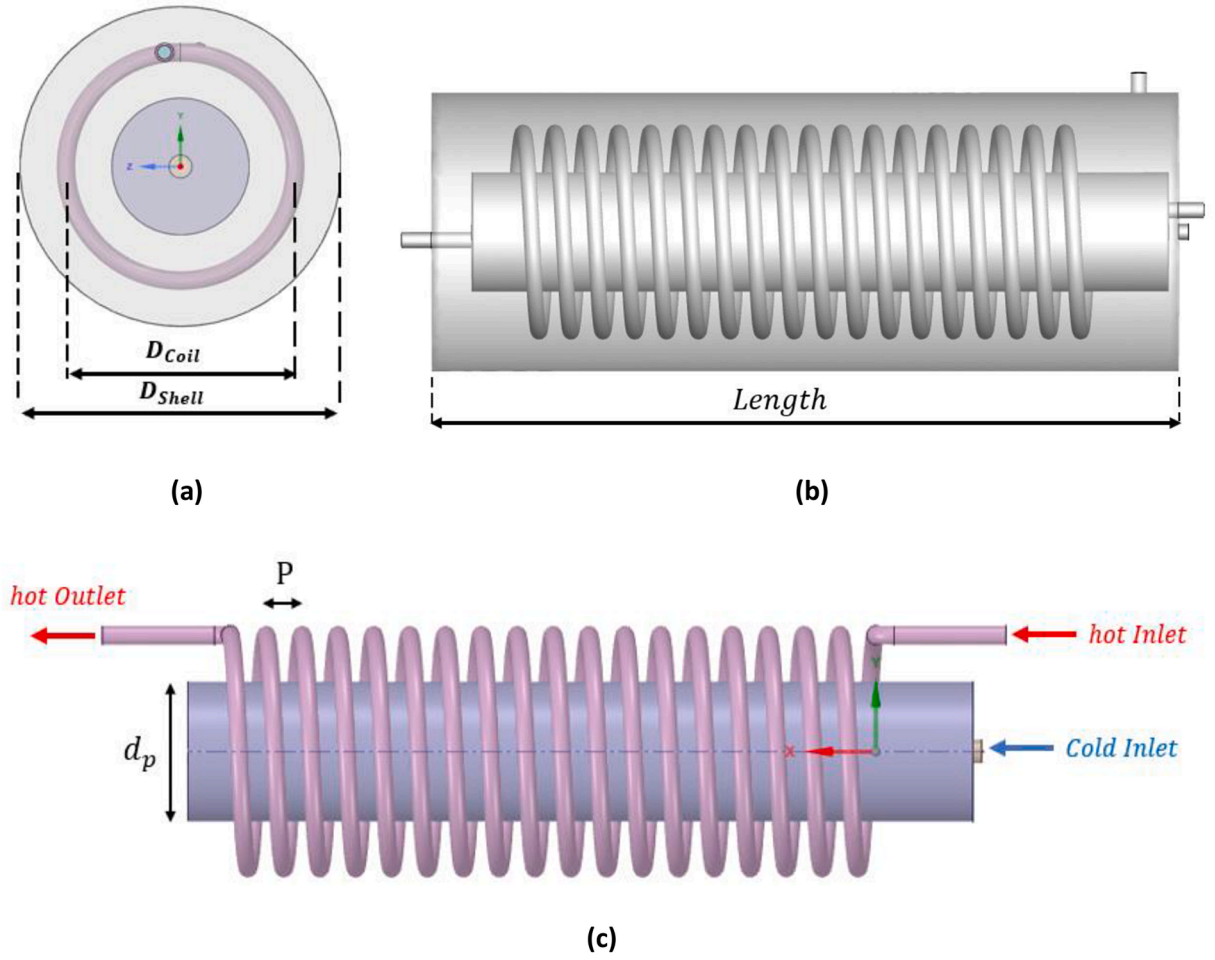

Figure (1). Schematics of the computational domain.

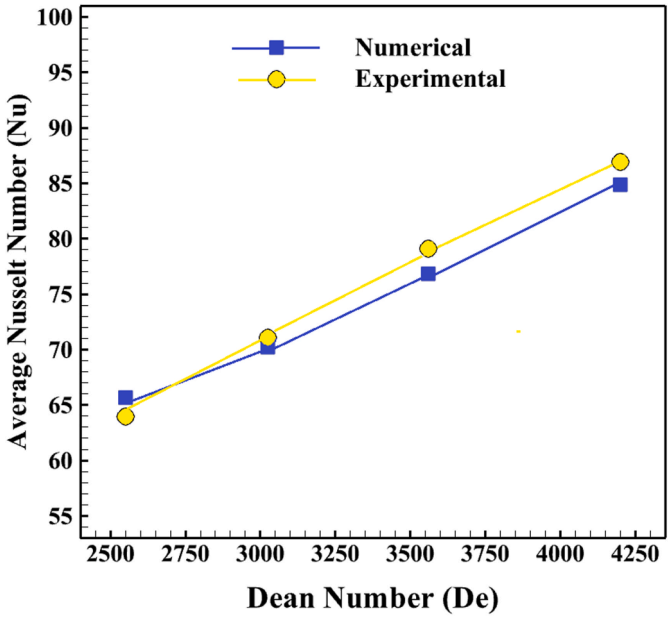

Figure (2). The results of the validation tests carried out on the current numerical model.

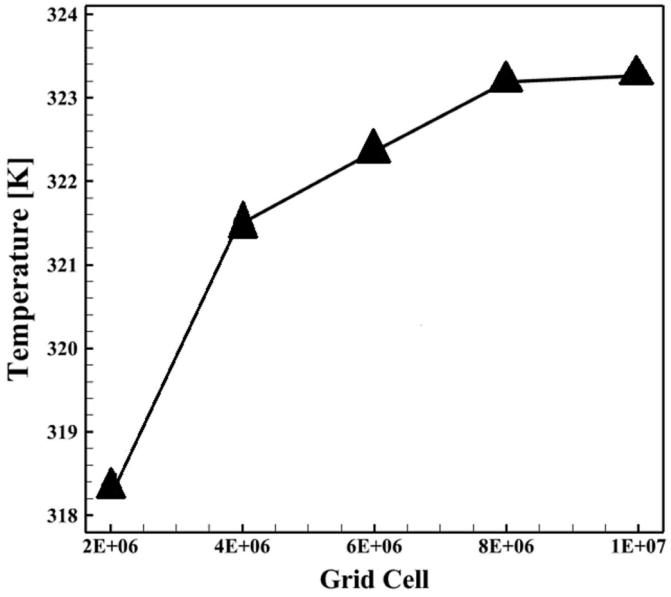

Figure (3). Mesh independence study for outlet temperature.

around enhancing turbulence and heat transfer, which can elevate fluid temperature through increased planes of transfers and vortex formation. Focusing on turbulent flows within the curved tube of a solar collector, the research examines the effects of two distinct spring inserts with varying spacings on flow dynamics [4]. M. Paikar and colleagues [5] investigated how utilizing turbulators of different shapes affected the overall heat transfer coefficient (HTC) and flow pressure drop. The findings indicated that the single and double-blade turbulators (SBT and DBT) raised the heat transfer coefficient (HTC) and pressure drop (PD) inside the tubes of the Shell and Tube Heat Exchanger (STHE). A.K. Rostami et al. [6] studied the finned tube heat exchanger with a shell and helical coil configuration. The findings indicate that the average Nusselt number remains constant on the coil side across all geometries, with minimal impact from Reynolds number variations on either side. In a study by M. Javidan et al. [7], heat storage in a heat exchanger using eccentric pipes and melting Paraffin RT50, an organic substance, was explored. The study focuses on heat transfer in a heat exchanger incorporating paraffin phase change material, explicitly determining the latent heat energy efficiency of the RT50 substance. M.A. Erfani Moghaddam and colleagues [8] investigated the incorporation of metal foam and fins in a triple concentric tube heat exchanger to examine the evolution of the melting process. Danial Salehipour and colleagues [9] studied the effectiveness of a spiral geometry

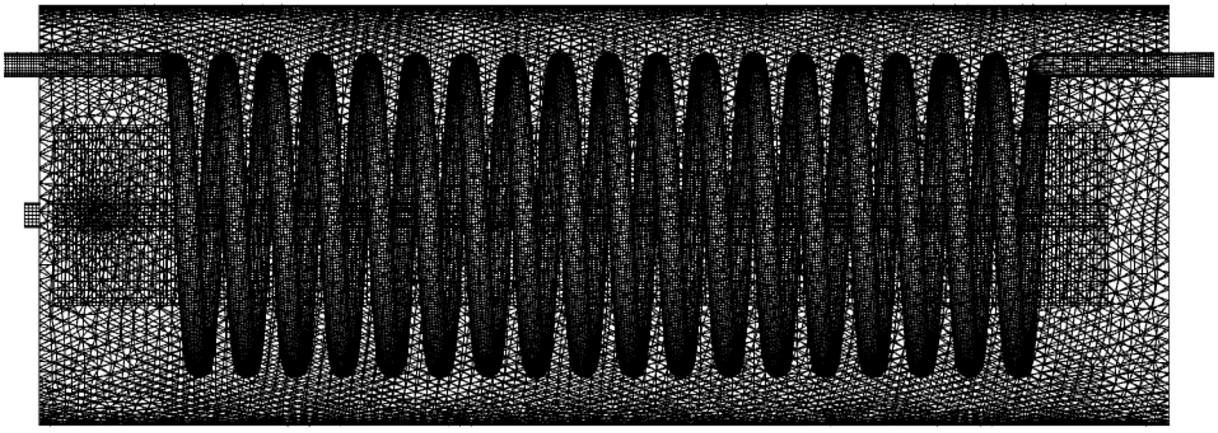

(a) In the Ansys Fluent software, mesh geometry

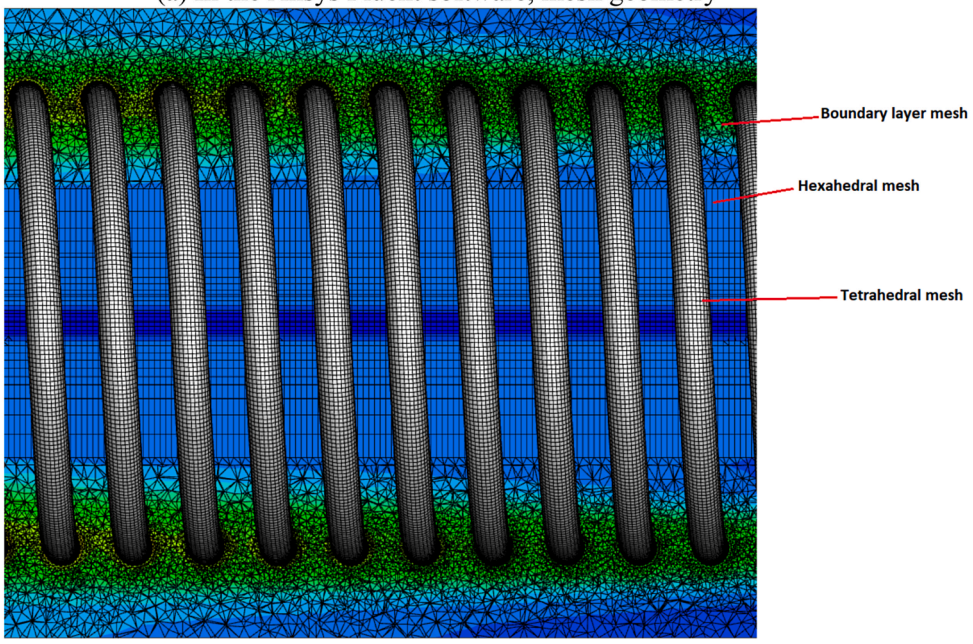

(b) The details of the meshed geometry in AnsysFluiont software

Figure (4). For the proposed model, a grid has been produced.

Table 2
The thermophysical properties of the working fluid and coil (steel).

Property	*Water*	*Water/Cuo_MOS$_2$(∅ = 0.3%vol)*	*Water/Zno_Al$_2$O$_3$(∅ = 0.3%vol)*
ρ [Kg/m^3]	998.2	1029.915	1016.534
Cp [j/Kg – K]	4182	4172.265	4176.429
k [w/m – K]	0.6	0.6072	0.60654
μ [Kg/m – s]	0.001003	0.001010	0.001010

economizer. Their research showed that in the third scenario, the cold-water outlet temperature was 2.85 % higher than in the first scenario. Additionally, the third scenario exhibited a maximum improvement of 1.39 % compared to the second scenario. This research [10] uses a local thermal non-equilibrium (LTNE) model to examine heat transfer processes in a porous fin, considering natural convection and radiation influences. The study shows that lowering the Rayleigh and Biot numbers decreases the temperature profiles of the solid phase. Furthermore, the temperature difference between the solid and fluid phases diminishes with a low Rayleigh and a high Biot number. Saeed Dinarvand and colleagues [11] examined the impact of an oblique magnetic field and temperature-dependent thermal conductivity to reduce the heat transfer rate. The findings indicate that incorporating temperature-dependent thermal conductivity and an oblique magnetic field decreases heat transfer. The reference research [12] investigates the transient per-

Table (3)
Specifications of the network related to the mesh specification.

Mesh specification	
Method:	Patch Conforming, Tetrahedrons
Body Size Type:	Element Size
Size Function:	Curvature, square
Quality:	Medium
Medium Mesh:	Element Size: 0.5 mm
	Nodes: 1414496
Fine Mesh:	Elements: 1518981
	Nodes: 1618221

Table (4)
Characteristics of mixed nanofluids ***Water/Zno_Al$_2$O$_3$*** with different volume percentages.

Property	*Water*	*Water/Zno_Al$_2$O$_3$(∅ = 0.1%vol)*	*Water/Zno_Al$_2$O$_3$(∅ = 0.3%vol)*	*Water/Zno_Al$_2$O$_3$(∅ = 0.5%vol)*
ρ [kg/m^3]	998.2	1003.661	1016.534	1033.789
Cp [j/kg – k]	4182	4178.421	4176.429	4165.210
k [w/m – k]	0.6	0.6059	0.60654	0.62139
μ [Kg/m – s]	0.001003	0.0010025	0.001010	0.0010126

formance of a solar power facility equipped with a parabolic receiver across different locations in Iran (6 cities). It evaluates the influence of integrating a latent heat storage system within the setup. Among the phase change agents (PCM) considered, $NaNO_3$ exhibited the best performance in the latent heat storage system, while H250 showed the weakest performance. A grooved spiral wound heat exchanger (GSWHE) was recommended to improve the heat transfer efficiency of the spiral wound heat exchanger. An experimental test setup was established to assess the heat transfer efficiency by comparing the performance of a spiral wound heat exchanger (SWHE). When water flow rates are reduced, the GSWHE's overall heat transfer coefficient is higher than that of the SWHE. The Wilson plot method was used to determine the heat transfer coefficient on both sides. Compared to the empirical correlation, there is an error of approximately 30 % for the SWHE's heat transfer coefficient on its tube side. The findings also indicate an apparent enhancement in heat transfer on the shell side of the GSWHE due to the presence of grooves. The overall performance of GSWHE was 1.23 times higher than that of SWHE, considering efficiency as a parameter, as stated in Refs. [13–19]. In the research outlined in citation [20], numerical analysis is conducted on the heat transfer and fluid flow within a dual-coil heat exchanger featuring a novel swirl generator that integrates a curved structure within the inner channel (hot side). Moreover, a larger inner radius of the turbulator improves heat transfer rate and effectiveness. Numerical simulations shall assess the thermal performance of a hydraulic double solenoid tube heat exchanger with a spiral configuration. Reference 21 is based on a new vortex generator consisting of two parts: the outermost curved blades, which have 2 holes in the interior section, and the semicircular blade, with 2 holes in the inside part. The study discussed in Ref. [22] investigates the heat transfer and pressure drop properties of a cone helically coiled tube heat exchanger using MWCNT/water nanofluids. The study indicates that, even 45 days after preparation of MWCNT Water nanofluids, they are stable and have not produced significant nanotubes in the inner walls of the tubes. This document introduces a numerical method for approximating partial differential equations that describe a common magnetic problem using the Spectral Element Method (SEM). This approach is believed to be the first of its kind [23]. This paper explores domain decomposition utilizing the principles of the Perfectly Matched Layer (PML) through the Spectral Element Method (SEM) for the first time. This method aims to efficiently solve near and far electromagnetic fields with minimal computational resources [24]. This research centers on utilizing an artificial neural network (ANN) to identify the most effective parameter values for heat transfer in a mixed convection process. The initial phase of the study involved performing Computational Fluid Dynamics (CFD) simulations to analyze the effects of different Grashof numbers [25]. Combined heat and power systems offer notable benefits in the present energy crisis scenario [26]. One of the key components frequently employed in such systems is the spiral heat exchanger (SHE). Several significant failure modes (FMs) exist that can reduce the efficiency of these devices [27] (see Table 1).

This research employed a uniquely designed shell and spiral tube heat exchanger to enhance efficiency. Additionally, ANSYS FLUENT, a computational fluid dynamics (CFD) software, was utilized to anticipate the target converter's thermohydraulic performance and heat transfer attributes. This included parameters such as convective heat transfer coefficient and friction coefficient. The main aim of the simulation in this study is to determine the suitable nanohybrid fluid for the spiral shell and tube heat exchanger to achieve enhanced thermal efficiency.(See Table 2)

2. Governing equations and boundary conditions

The equations dictating mass, momentum, and energy conservation can be formulated as follows [20,21]:

$$\frac{\partial \rho}{\partial t} + \nabla . \left(\rho \vec{v}\right) = 0 \tag{1}$$

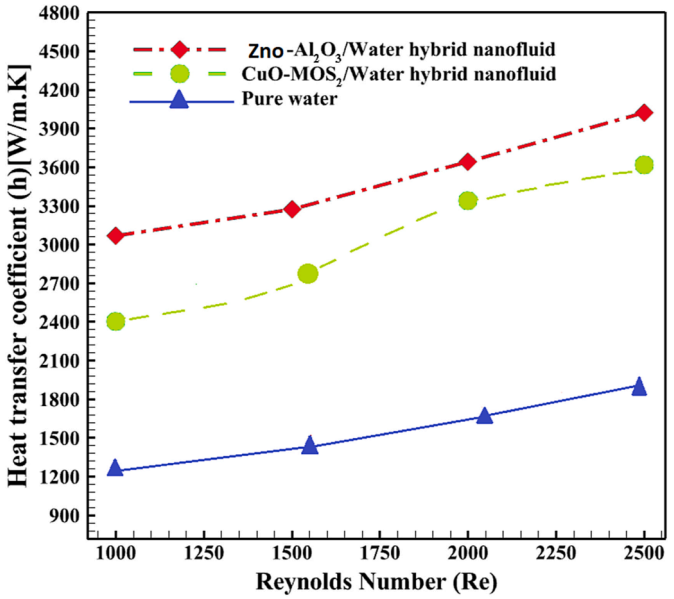

Figure (5). Changes in convective heat transfer coefficient at various Reynolds numbers for the fluid flowing through the spiral coil.

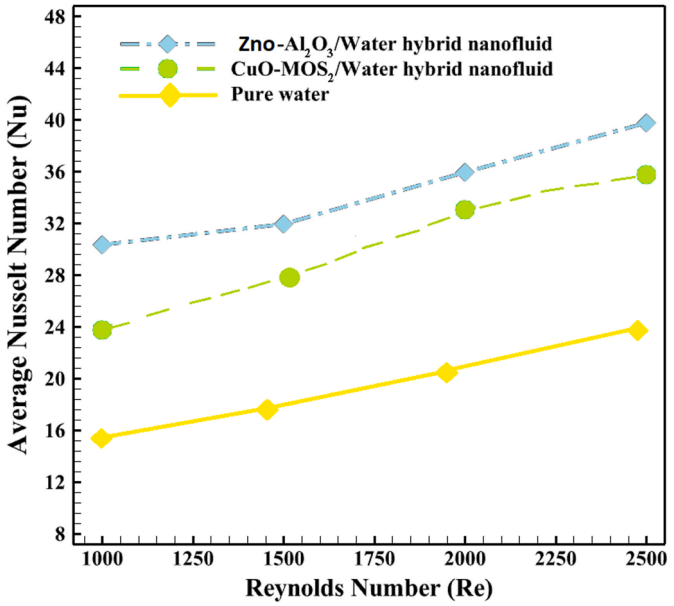

Figure (6). Changes in the Nusselt number based on convective heat transfer coefficient at various Reynolds numbers for the fluid passing through.

$$\frac{\partial\left(\rho\vec{v}\right)}{\partial t}+\nabla.\left(\rho\vec{v}\vec{v}\right)=-\nabla p+\nabla.\left(\mu\nabla\vec{v}\right) \tag{2}$$

$$\frac{\partial\left(\rho c_p T\right)}{\partial t}+\nabla.\left(\vec{v}\left(\rho c_p T\right)\right)=\nabla\left(k\nabla T\right) \tag{3}$$

Here, ρ, μ, k, and Cp denote the density, viscosity, thermal conductivity, and heat capacity of the working fluid. Additionally, T, v, and (P) represent the temperature, velocity, and pressure, respectively. The average Nusselt number (Nu_{ave}), friction factor (f), and overall performance (η) are defined as follows [20,21]:

$$Nu_{ave}=\frac{h_m d_h}{k} \tag{4}$$

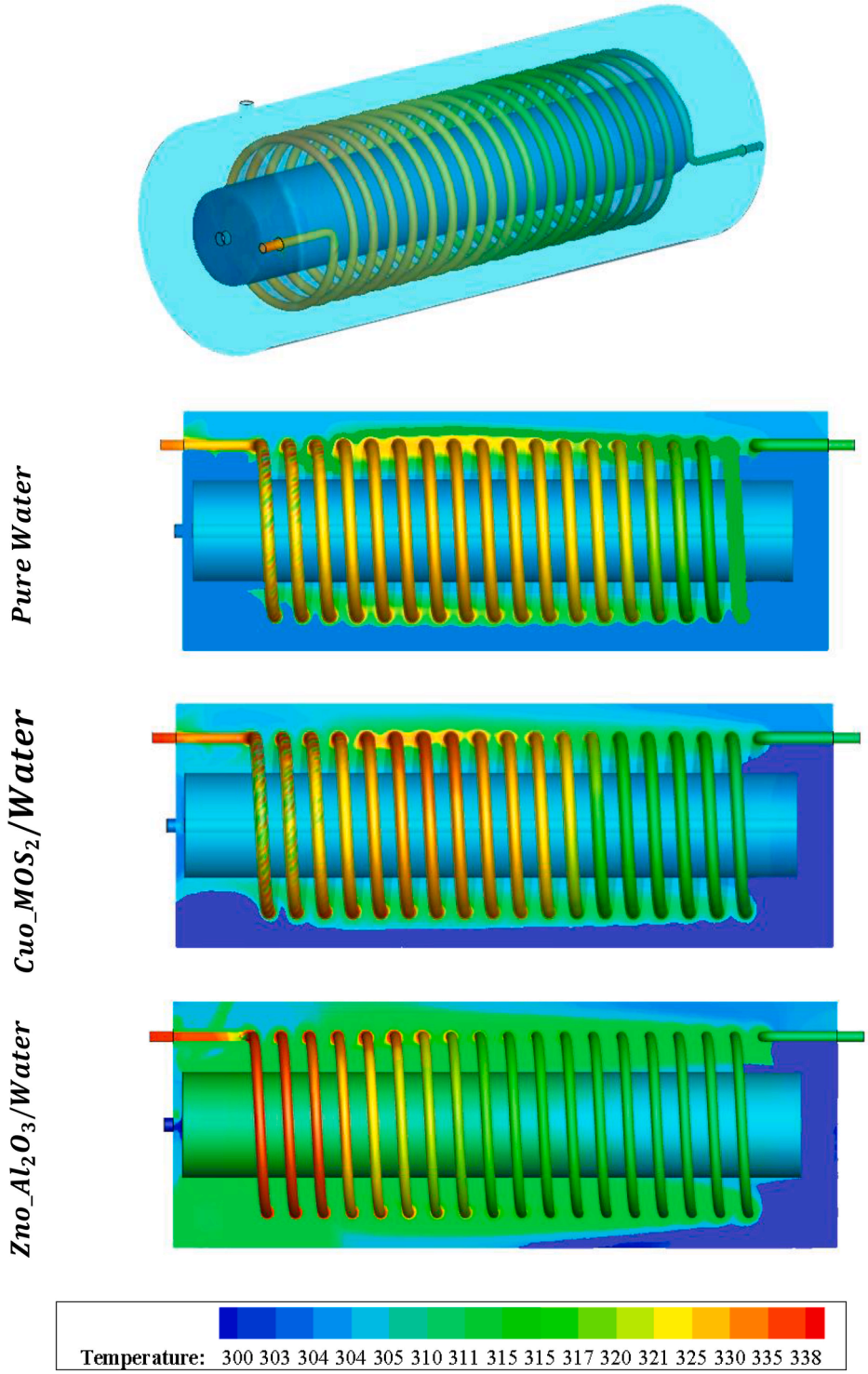

Figure (7). State of heat transfer between two fluids.

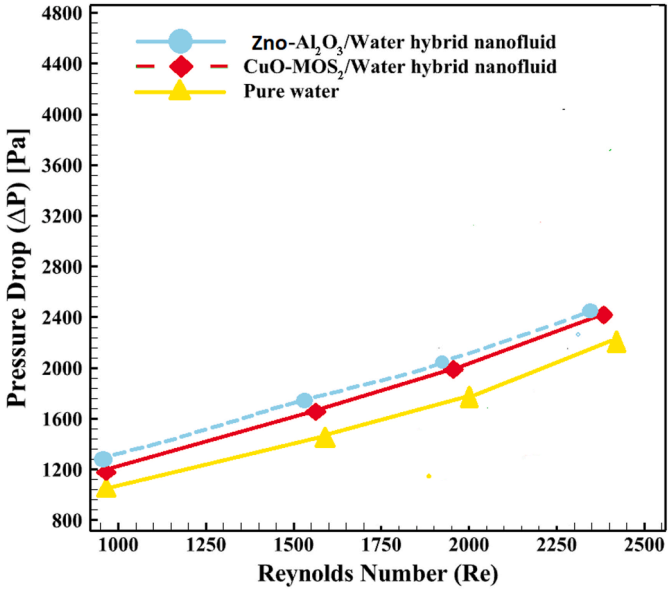

Figure (8). Pressure drop changes for three types of working fluid.

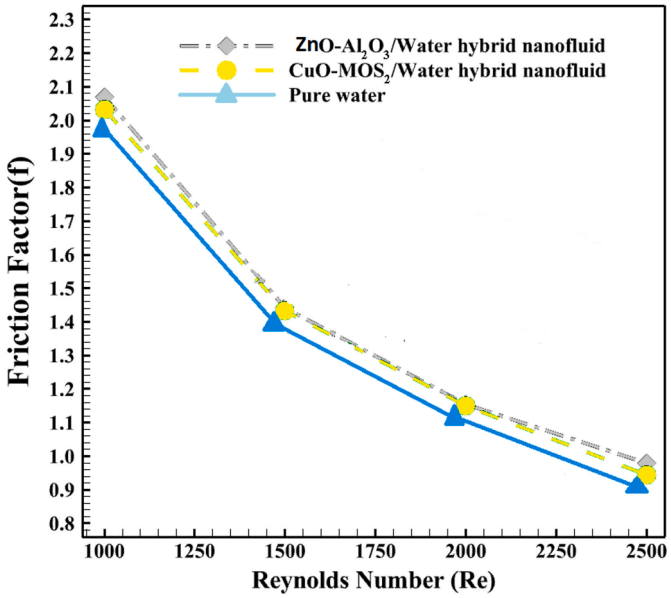

Figure (9). Friction coefficient changes for three types of working fluid.

$$f = \frac{2d_h \Delta p}{\rho u^2 L} \tag{5}$$

$$\eta = \left(\frac{Nu}{Nu_0}\right)\left(\frac{f_0}{f}\right)^{\frac{1}{3}} \tag{6}$$

Here, d_h and L represent the diameter and hydraulic length of the pipe, respectively. H_m denotes the average convective heat transfer coefficient, where the subscript 0 signifies the flow mode of the base fluid (water). Δp represents the pressure drop. The critical Reynolds number in the spiral tube can be calculated using a specific correlation formula, which is:

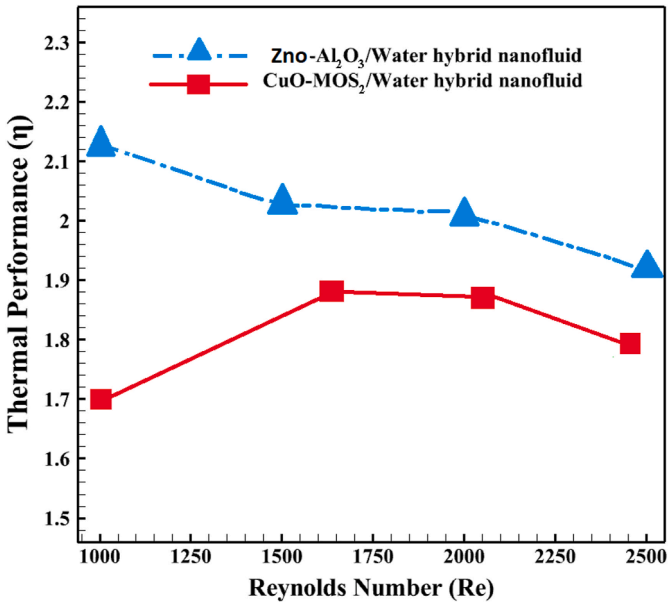

Figure (10). To determine the best converter mode, changes in the thermal performance coefficient shall be taken into account.

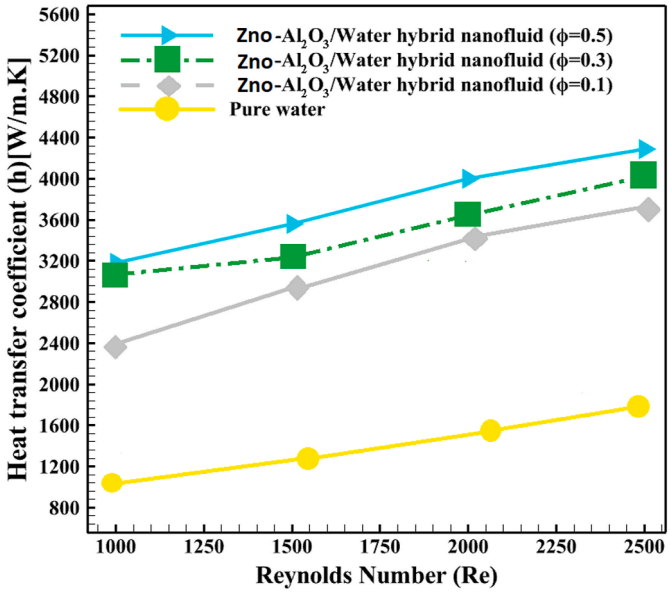

Figure (11). The influence of particle concentration on the convective heat transfer coefficients.

$$Re_{cr} = 2300\left[1 + 8.6\left(\frac{r}{R_c}\right)^{0.45}\right] \tag{7}$$

Here, r and R_C represent the pipe and coil ring radii, respectively. In this study, r = 3 mm and RC = 50 mm. Using Equation (7), the critical Reynolds number Re_{cr} = 7877 can be calculated for this situation. Additionally, the critical Reynolds number proposed by Ito [21] is:

$$Re_{cr} = 20000\left(\frac{r}{R_c}\right)^{0.32} \tag{8}$$

This article utilizes water as the base fluid and incorporates four hybrid nanofluids containing copper, molybdenum disulfide, aluminum oxide, and zinc. These nanofluids are mixed with water at a specific volume percentage of 0.3 %, and a unique chemical com-

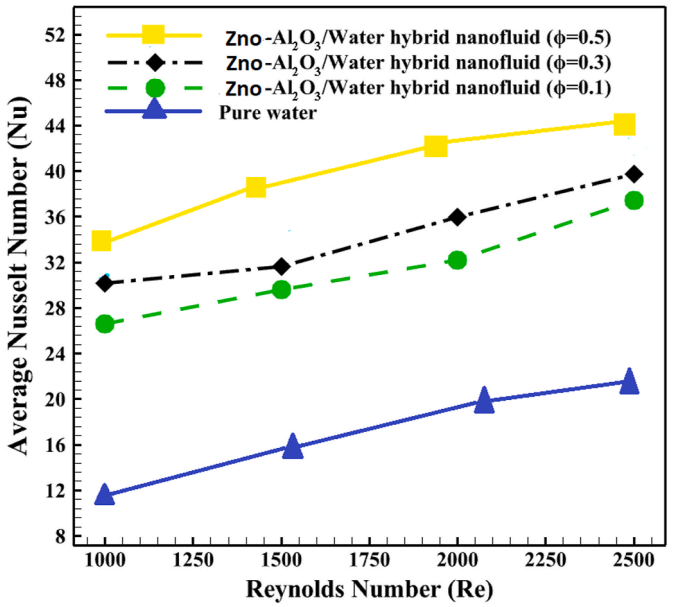

Figure (12). The effect on Nusselt number of the volume concentration of the desired fluid nanohybrid.

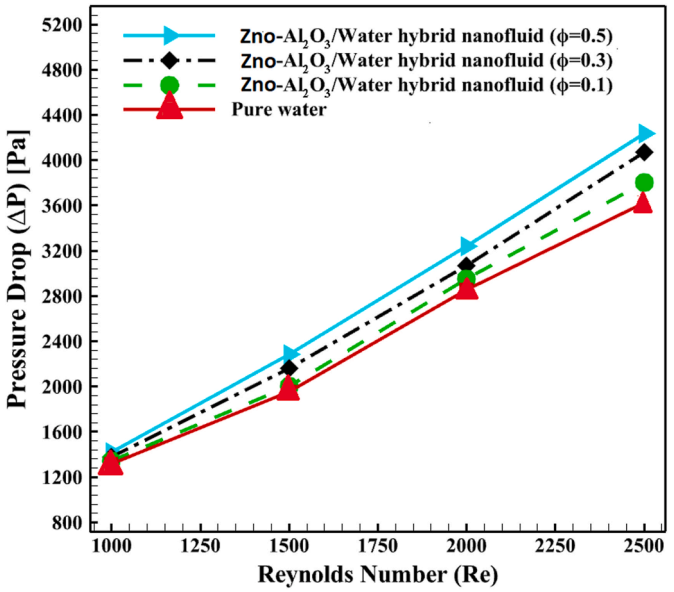

Figure (13). Changes in value of pressure drop due to the volumetric concentration of nanohybrid.

position is employed in the geometry discussed in the article. This specific hybrid nanofluid is selected for its elevated heat capacity, which enhances the thermal efficiency of the converter, and its high mass-to-volume ratio. Additionally, their solubility in the base fluid makes them a preferred option for utilization.

$ZnO\_Al_2O_3$ nanoparticles dispersed in water at volume concentrations ranging from 0.1 % to 0.5 % serve as the heating medium within the spiral tubes. The density and specific heat of the nanofluid were calculated using Eqs. (9) and (10) based on the mixture rules. The thermal conductivity and viscosity of the nanofluid were predicted using two empirical correlations introduced by Corcione [25] (Equation (11) and (12)). In Equations (9)–(12), the temperature-dependent thermo-physical properties of water were incorporated.

$$\rho_{nf} = (1-\varphi_p)\,\rho_f + \varphi_p \rho_p \tag{9}$$

$$(\rho C_p)_{nf} = (1-\varphi_p)\,(\rho C_p)_f + \varphi_p (\rho C_p)_p \tag{10}$$

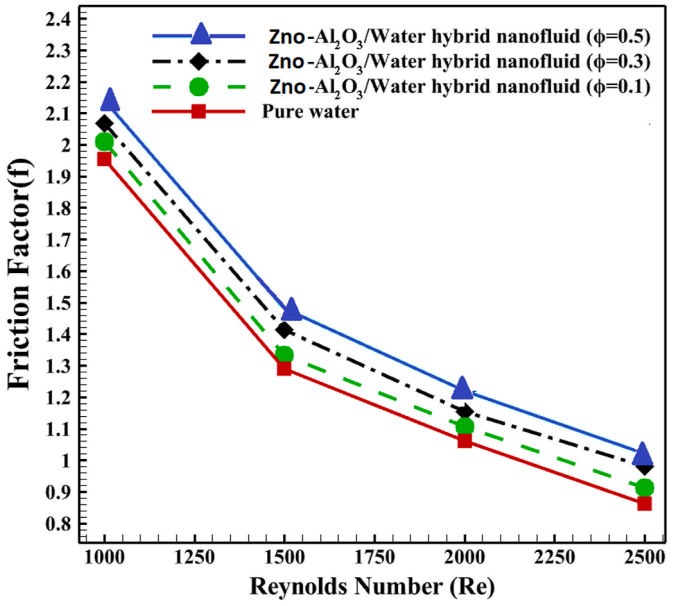

Figure (14). Changes in friction factor value based on volumetric concentrations of fluid nanohybrid.

$$\frac{\lambda_{nf}}{\lambda_f} = 1 + 4.4 Re_{br}^{0.4}\, Pr^{0.6} \left(\frac{T}{T_{fr}}\right)^{10} \left(\frac{\lambda_p}{\lambda_f}\right)^{0.03} \varphi_p^{0.6} \tag{11}$$

$$\frac{\mu_{nf}}{\mu_f} = \frac{1}{1 - 34.87 \left(\frac{d_p}{d_f}\right)^{-0.3} \varphi_p^{1.03}} \tag{12}$$

$\rho_{\ nf}$ is the density of nanofluid particles, ρ_f is the density of the base fluid, φ_p is the fluid concentration, ρ_p is the density of the fluid,Cp is the specific heat, λ_{nf} is the thermal conductivity of nanofluid, Re is the Reynolds number, Pr is the Prandtl number, T_{fr} is the temperature of the freezing point of the base fluid, λ_p is the thermal conductivity of particle, μ_{nf} is the viscosity of nanoparticles, and d_p is the tube diameter (see Fig. 1).

2.1. The studied geometry

As depicted in Fig. 2, this specific shell and tube converter configuration deviates from conventional designs. In this setup, a hollow tube is placed inside the shell, enabling the cold liquid to enter the shell through this tube. In simpler words, the cold fluid first enters the shell side's inner tube and then moves into the main shell, passing over the spiral coil. Eventually, it exits the shell, as shown in Fig. 2. This technique permits fluid flow regulation on the shell side, enhancing the converter's thermal efficiency.

2.2. Numerical procedure

This issue is addressed by solving it using the finite volume method in the ANSYS FLUENT 18.2 commercial computational simulation software. The distribution of mass, momentum and energy conservation equations is based on a Second Order Upwind scheme. The velocity-pressure coupling is managed using the SIMPLE algorithm. The Gradient Evaluation using the GreenGauss Cell Based Methodology is carried out. In addition, for residuals of continuity, momentum, and energy, the convergence criterion 10^{-6} is set.

2.3. Verification investigation of employed numerical model

Careful alignment of geometrical conditions and equations to the problem is vital for a numerical model to be validated effectively. The above numerical method was applied by comparing the Nusselt number for flow within the conical coiled tube at different Reynolds numbers, referencing a relevant article [21]. The Dean number and the mean Nusselt numbers shall be determined as follows:

$$D_e = Re \times \left(\frac{d_i}{2 \times R_c}\right)^{0.5} \tag{13}$$

$$Nu_i = \left(\frac{h_i \times d_i}{k}\right) \tag{14}$$

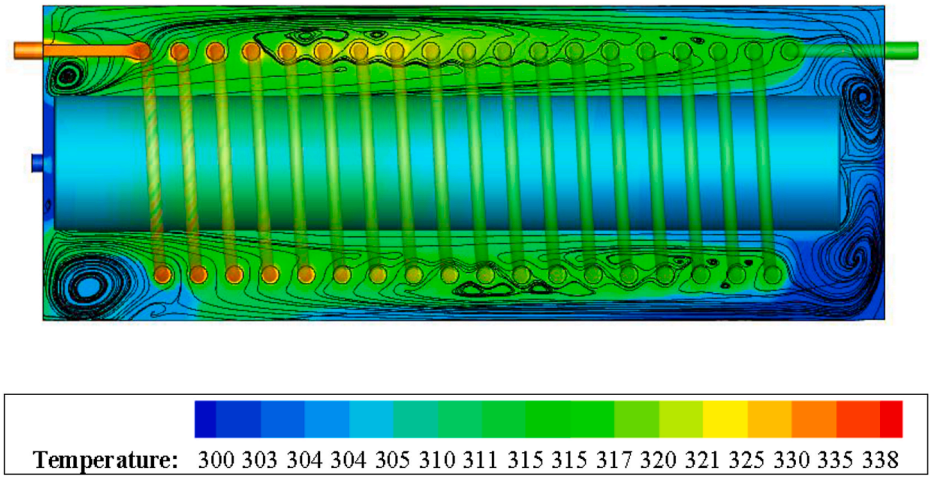

Figure (15). The process of fluid movement in the desired exchanger and heat transfer between two fluids.

The heat transfer within the internal spiral tubes and the corresponding formula for heat transfer can be determined as per the following equation:

$$Q = h_i \times A_i \times \left(T_{Wall} - T_{bulk}\right) \tag{15}$$

Corresponding to the boundary condition of the outer wall of the heat exchanger:

$$T_w = 0 \tag{16}$$

Fig. 2 illustrates the results of a validation analysis for this numerical model. The numerical outcomes from the present model are contrasted with the experimental findings [22]. For each Reynolds number, the numerical results of the problem-solving are compared with experimental data. The validation outcomes show a reasonable error margin, demonstrating the reliability of the numerical model for validation purposes.

3. Mesh independency study

A grid independence study is necessary to determine the optimal size of the network and improve its cost and time effectiveness. This research selected six grids with cell counts of 2000058, 4952861, 6731068, 8932518, and 10165818 for assessment. Fig. 3 gives an overview of the results (see Fig. 4).

Table 3 displays the attributes of mesh distribution on the problem's geometry (see Table 4).

3.1. Relevant boundary conditions in the studied geometry

A hot fluid flow, including hybrid and nonhybrid nanofluids, flows into the spiral tube at the inlet boundary. Different Reynolds numbers, particularly 1000, 1500, 2000, and 2500, are applied to the hot fluid. At the same time, a constant Reynolds number of 1500 keeps cold water flowing freely into the shell. Output pressure type shall be defined as the output boundary condition for the spiral coil and the shell.

3.2. Boundary conditions of the wall

The outer shell wall will be thermally insulated, whereas the inner wall of the spiral coil will be regulated to control the heat transfer within the tube.

4. Results and discussion

In this section, we will continue to analyze the results after reviewing the geometry studied and validating the present work. The results will be presented in various graphs and contour charts representing the different modes of action.

4.1. Exploring the impact of the working fluid type on heat transfer and pressure drop in the intended exchanger shell or tube

For fluid flowing through a designated spiral coil, the figure below shows variations in convective heat transfer coefficient at various Reynolds values. Three different types of working fluids with a volume concentration of 0.3 % shall be included in this evaluation.

As seen in the figure above, the lowest value of the convective heat transfer coefficient is linked to a Reynolds number of 1000, whereas the highest value is connected to a Reynolds number of 2500. This diagram demonstrates that raising the Reynolds number enhances any fluid's vortex heat transfer coefficient. Moreover, the nanohybrid fluid Water/ZnO_Al_2O_3 demonstrates the highest con-

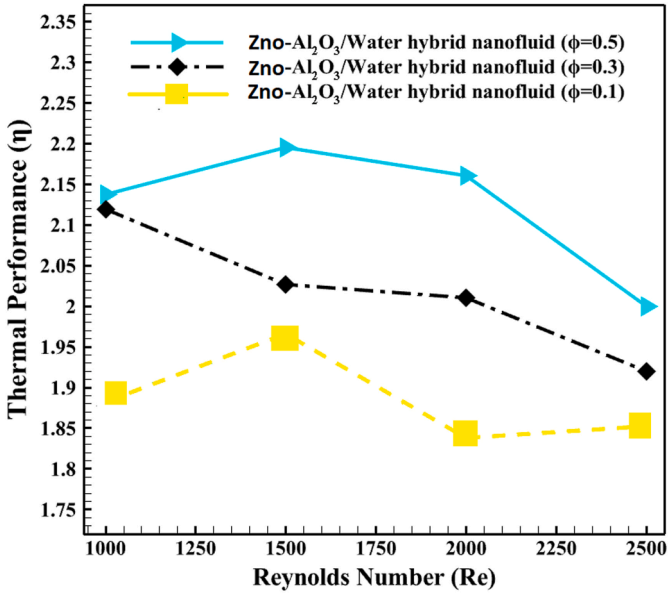

Figure (16). Variations in the thermal performance value depending on the volume concentrations of the fluid nanohybrid.

vective heat transfer coefficient, indicating superior heat transfer efficiency between the two fluids with this particular nanofluid (see Fig. 5).

The figure below (Fig. 6) illustrates variations in the Nusselt number, dependent on the convective heat transfer coefficient at different Reynolds numbers for the fluid flowing through the specified spiral coil. This examination involves three distinct types of working fluids.

This examination involves the three mentioned earlier; this figure shows that the fluctuations in the Nusselt number align with those of the convective heat transfer coefficient. The Nusselt number also increases when Reynolds' numbers are increased—e distinct types of working fluids. In addition, the nanohybrid fluid Water/Zno_Al_2O_3 appears to have the highest Nusselt value, while the base fluid Water/Zno_Al_2O_3 appears to have the lowest value. This implies that, when using Water/Zno_Al_2O_3 fluid nanohybrid, the heat transfer efficiency from one liquid to another is improved and these differences can be seen in the temperature distribution as described below:

The best heat transfer between the two fluids occurs when the fluid nanohybrid Water/Zno_Al_2O_3 is used, as shown in Fig. 7 above. In this figure, the hot fluid has absorbed more heat than the cold fluid, decreasing temperature. Fig. 8 below depicts the changes in pressure drop for three types of working fluids within the $1000 < Re < 2500$ range.

The above chart shows an increasing trend with fluid nanohybrid changes, different Reynolds numbers, and a decrease in pressure. The data indicates that the pressure drop for the two nanohybrid fluids is elevated compared to the base fluid, water. This can be attributed to the increased viscosity of nanohybrid fluids compared to the base fluid. Additionally, the figure suggests that the peak pressure drop linked to the nanohybrid fluid Water/Zno_Al_2O_3 is observed at a Reynolds number of 2500. Indeed, a heightened pressure drop will result in greater energy consumption from the pump or necessitate increased pumping effort.

The diagram below (Fig. 9) displays the changes in the friction coefficient for three types of working fluids within the $1000 < Re < 2500$ range.

Fig. 9 above shows lower Reynolds numbers and fluid velocities are associated with higher friction coefficients. Moreover, it is clear that with an increase in fluid velocity, the friction coefficient decreases due to their inverse relationship, along with the quicker escape of fluid from inside the tube and reduced contact of the fluid with the inner surface of the tube. The highest friction coefficient value is linked to the nanohybrid fluid Water/Zno_Al_2O_3.

Fig. 10 shows the differences between the thermal efficiency coefficients used as measurements to determine the converter's optimum performance mode.

According to the figure above, using the Water/Zno_ Al_2O_3 fluid nanohybrid is recommended for improved efficiency in the intended shell and tube heat exchanger. It is also observed that beyond a Reynolds number of 1500, the heat exchanger efficiency will decrease when both types of fluid nanohybrid are utilized. In addition, according to the figure above, Reynolds number 1000 is associated with a fluid nanohybrid Water/Zno _Al_2O_3 and constitutes the peak thermal efficiency of the targeted converter. The converter efficiency shall be 21 % higher than that of the Water/Zno_Al_2O_3 fluid nanohybrid at the lowest Reynolds number when using the Water/Zno_Al_2O_3 fluid nanohybrid.

Table (5)
Comparison of the ratio of combined nanofluids Zno_Al_2O_3 at different temperatures and volume percentages.

Temperature	Density ratio of Zno_Al_2O_3 nafluid in different volume concentration		
	φ = 0.1	φ = 0.3	φ = 0.5
300	1.1084	1.1278	1.1676
310	1.0954	1.1123	1.1590
315	1.0884	1.0911	1.1055
323	1.0639	1.0799	1.0902

4.2. Exploring the impact of the volume concentration of Water/Zno_Al_2O_3 nanohybrid fluid on heat transfer and pressure drop in the desired converter

In this section of the review, we will examine how the volume concentration of the Water/Zno_Al_2O_3 nanohybrid fluid influences the factors that affect the efficiency of the desired converter. In the following figure, the impact of the volume concentration of the target fluid nanohybrid on the convective heat transfer coefficient is depicted as one of the indicators of heat transfer.

Above, Fig. 11 illustrates the impact of particle concentration on the convective heat transfer coefficient. The Reynolds number is directly correlated with the convective heat transfer coefficient increase. The maximum heat transfer coefficient shall be achieved in nanohybrid fluid with a volume concentration of 0.5 %. The incorporation of Zno_ Al_2O_3 further enhances the thermal conductivity of nanofluids. Moreover, the incorporation of ZnO–Al_2O_3 nanoparticles delays the formation of the thermal boundary layer, enhancing heat transfer between the two fluids. Fig. 12 displays the impact of the volume concentration of the target fluid nanohybrid on the Nusselt number as a critical indicator of heat transfer.

The value of the Nusselt number increases as the Reynolds number and particle volume increase. Significant increases in the number of Nusselt compared to water at volume concentrations of 0.1 %, 0.3 %, and 0.5 % nanofluid hybrid Water_Al_2 O_3 are observed. The enhancement in heat transfer results from thoroughly mixing water particles and Zno_Al_2O_3. In addition, the turbulent motion of Zno_Al_2O_3 particles in base fluid disrupts formation of boundary layers and promotes secondary flows. The internal convective heat transfer coefficient is directly correlated with the Nusselt number. Additionally, the Nusselt number increases as the convective heat transfer coefficient and volume concentration are elevated. This is attributed to the enhanced heat transfer between the two fluids, as illustrated in the figure below:

The following Fig. 13 depicts the variations in the pressure drop value depending on the volume concentrations of the Water/ZnO_Al_2O_3 fluid nanohybrid at different Reynolds numbers.

The figure above illustrates the rising trend of pressure drop with alterations in the volume concentration of nanofluid particles and Reynolds number. Compared to base fluid, the pressure drop for nanofluids with concentrations of 0.1 %, 0.3 %, and 0.5 % is 5 %, 12 %, or 15 % higher. The presence of additional ZnO_ Al_2O_3 particles causes the increased viscosity. It is also evident that the peak pressure drop associated with the desired nanohybrid fluid happens at a volume concentration of 0.5 % and a Reynolds number of 2500. The change in friction coefficient according to the various volumetric concentrations of Water and ZnO_Al_2O_3 nanohybrid fluid, broken down by Reynolds number, can be found below Fig. 14.

The figure above illustrates the declining pattern of the friction coefficient with variations in the Reynolds number. Additionally, it is noted that the friction coefficient value rises with an increase in the volume concentration of the nanohybrid fluid. This phenomenon results from the increased viscosity and the presence of more ZnO_Al_2O_3 particles. Additionally, the highest friction coefficient is observed at a volume concentration of 0.5 % and a Reynolds number of 1000, attributed to the lower velocity and enhanced contact of the fluid with the pipe walls. An example of how the fluid moves from one liquid to another in a desired exchanger and heat transfer shall be shown in Fig. 15.

As depicted in the above figure, the cold fluid flows through the section within the pipe between the spiral coils; this absorbs some heat from the spiral coil during this passage. Subsequently, the fluid exits the pipe end and impacts the shell wall, inducing a rotational motion. Heating should primarily take place between the two fluids. The figure below illustrates variations in the thermal performance coefficient, representing the optimal performance mode of the desired converter for different volume concentrations of the water/ZnO_Al_2O_3 nanohybrid fluid.

As per the above figure, utilizing a water/ZnO_Al_2O_3 fluid nanohybrid with a volume concentration of 0.5 % is recommended to achieve higher efficiency from the desired shell and tube heat exchanger. It is also evident that employing volume concentrations above 0.1 % at the lowest Reynolds number enhances the converter's efficiency under consideration. However, at the highest Reynolds number (2500), the efficiency of the nanohybrid fluid with concentrations of 0.5 % and 0.3 % decreases, while for the fluid with a concentration of 0.1 %, the efficiency increases. Furthermore, as depicted in the figure above (Fig. 16), the desired converter's peak thermal efficiency occurs at a Reynolds number of 1500, associated with the water/ZnO_Al_2O_3fluid nanohybrid at a volume concentration of 0.5 %.

Table 5 displays the density ratio of ZnO–Al_2O_3 mixed nanofluid at various temperatures and volume percentages. The findings indicate that as the volume percentage of nanofluids rises, along with enhanced heat transfer, the nanofluid ratio also increases.

5. Conclusion

This research employed a uniquely designed shell and spiral tube heat exchanger to enhance efficiency. Furthermore, the computational fluid dynamics (CFD) software ANSYS FLUENT was used to forecast the converter's thermohydraulic performance and heat transfer characteristics, encompassing factors like the convective heat transfer coefficient and friction coefficient. The main objective of the simulation in this study is to determine the most suitable nanohybrid fluid for the spiral shell and tube heat exchanger to achieve enhanced thermal efficiency. Examples of the acquired results are illustrated below:

- A significant factor influencing the thermohydraulic performance of shell and spiral tube heat exchangers has also been shown to be the type of fluid nanohybrid selected.
- The maximum thermal efficiency of the specified converter is observed at Reynolds number 1000 and linked to the fluid nanohybrid Water/ZnO_Al_2O_3.
- Out of the three chosen fluid nanohybrids in the simulation, it was observed that the Water/ZnO_Al_2O_3 fluid nanohybrid exhibits superior thermal performance compared to the other fluids.

CRediT authorship contribution statement

Naim Ben Ali: Conceptualization, Formal analysis, Writing – review & editing. **Dheyaa Jumaah Jasim:** Methodology, Writing – review & editing. **Saman Aminian:** Formal analysis, Software. **Pradeep Kumar Singh:** Investigation, Validation. **Husam Rajab:** Investigation, Resources, Software. **Ismail M.M.Elsemary:** Data curation, Writing – review & editing. **Lioua Kolsi:** Data curation, Resources, Writing – review & editing. **Neaman Sohrabi:** Visualization, Validation, Supervision, Software, Resources. **Reza Haddadvand:** Writing – review & editing, Writing – original draft, Investigation. **Seyyed Amirreza Abdollahi:** Formal analysis, Data curation, Conceptualization.

Declaration of competing interest

The authors declare that they have no known competing financial interests or personal relationships that could have appeared to influence the work reported in this paper.

Data availability

Data will be made available on request.

Acknowledgments

The authors extend their appreciation to the Deanship of Scientific Research at Northern Border University, Arar, KSA for funding this research work through the project number “NBU-FPEJ-2024-2907-01".

References

[1] S.M. Kim, J.H. Jo, Y.E. Lee, Y.S. Yoo, Comparative study of shell and helically-coiled tube heat exchangers with various dimple arrangements in condensers for odor control in a pyrolysis system, Energies 9 (12) (Dec. 2016) 1027, https://doi.org/10.3390/en9121027.
[2] A. Alimoradi, M. Olfati, M. Maghareh, Numerical investigation of heat transfer intensification in shell and helically coiled finned tube heat exchangers and design optimization, Chem. Eng. Process. Process Intensif. 121 (Nov. 2017) 125–143, https://doi.org/10.1016/j.cep.2017.08.005.
[3] As’ ad Alizadeh, et al., Numerical investigation of the effect of the turbulator geometry (disturber) on heat transfer in a channel with a square section, Alex. Eng. J. 69 (2023) 383–402 https://doi.org/10.1016/j.aej.2023.02.003, .
[4] Peng Yin, et al., Evaluation of efficiency, thermohydraulic performance evaluation criterion, and field synergy principle improvement of the parabolic solar collector containing the hybrid nanofluid using spring turbulators, Case Stud. Therm. Eng. 41 (2023) 102571, https://doi.org/10.1016/j.csite.2022.102571.
[5] M. Paikar, et al., Hydrothermal assessment of a double-pass shell and tube heat exchanger in the presence of blade turbulators with different configurations, International Journal of Thermofluids 21 (2024) 100577, https://doi.org/10.1016/j.ijft.2024.100577.
[6] A.K. Rostami, D.D. Ganji, Selecting superior fin geometry among four suggested geometries for shell and helically coiled finned tube heat exchangers with numerical simulation and experimental validation, Results in Engineering 17 (2023) 100867, https://doi.org/10.1016/j.rineng.2022.100867.
[7] M. Javidan, et al., Heat storage by melting the organic material of Paraffin RT50 in a heat exchanger with eccentric pipes, J. Energy Storage 54 (2022) 105280, https://doi.org/10.1016/j.est.2022.105280.
[8] MA Erfani Moghaddam, et al., Metal foam and fin implementation into a triple concentric tube heat exchanger over melting evolution, Theoretical and Applied Mechanics Letters 12 (2) (2022), 100332 https://doi.org/10.1016/j.taml.2022.100332, .
[9] Danial Salehipour, Bahram Jalili, Payam Jalili, Effect of humidification of combustion products in the boiler economizer with spiral geometry, Results in Engineering (2024) 101906, https://doi.org/10.1016/j.rineng.2024.101906.
[10] Payam Jalili, et al., Analytical and numerical investigation of heat transfer of porous fin in a local thermal non-equilibrium state, Heliyon (2024) e26424, https://doi.org/10.1016/j.heliyon.2024.e26424.
[11] Saeed Dinarvand, et al., Squeezing flow of aqueous CNTs-Fe3O4 hybrid nanofluid through mass-based approach: effect of heat source/sink, nanoparticle shape, and an oblique magnetic field, Results in Engineering 17 (2023) 100976, https://doi.org/10.1016/j.rineng.2023.100976.
[12] M. Hadi, et al., Simulation of a solar power plant with parabolic receivers in several parts of Iran in the presence of latent heat thermal energy storage system, Therm. Sci. Eng. Prog. 30 (2022), 101249 https://doi.org/10.1016/j.tsep.2022.101249, .
[13] M. Javidan, et al., Investigation of convection and radiation heat transfer of paraffinic materials and storage of thermal energy in melting process of PCMs in the cavity with transparent inner walls, Energy Rep. 8 (2022) 5522–5532, https://doi.org/10.1016/j.egyr.2022.04.025.
[14] M. Javidan, et al., Thermal energy storage inside the chamber with a brick wall using the phase change process of paraffinic materials: a numerical simulation, Theoretical and Applied Mechanics Letters 12 (3) (2022) 100329, https://doi.org/10.1016/j.taml.2022.100329.
[15] Zhongdi Duan, et al., Liquid-migration based model for predicting the thermal performance of spiral wound heat exchanger for floating LNG, Appl. Energy 206 (2017) 972–982, https://doi.org/10.1016/j.apenergy.2017.09.003.
[16] Yoshinori Itaya, et al., Heat and mass transfer through spiral tubes in absorber of absorption heat pump system for waste heat recovery, Propulsion and Power Research 6 (2) (2017) 140–146, https://doi.org/10.1016/j.jppr.2017.05.004.

[17] Simin Wang, et al., Optimization investigation on configuration parameters of spiral-wound heat exchanger using Genetic Aggregation response surface and Multi-Objective Genetic Algorithm, Appl. Therm. Eng. 119 (2017) 603–609, https://doi.org/10.1016/j.applthermaleng.2017.03.100.
[18] Jinxing Wu, et al., Numerical simulation and experimental research on the comprehensive performance of the shell side of the spiral wound heat exchanger, Appl. Therm. Eng. 163 (2019) 114381, https://doi.org/10.1016/j.applthermaleng.2019.114381.
[19] S. Bahrehmand, A. Abbassi, Heat transfer and performance analysis of nanofluid flow in helically coiled tube heat exchangers, Chem. Eng. Res. Des. 109 (March) (2016) 628–637 https://doi.org/10.1016/j.cherd.2016.03.022, 10.1016/j.cherd.2016.03.022.
[20] Karouei Hashemi, H. Seyed, S. Mousavi Ajarostaghi Seyed, Influence of a curved conical turbulator on heat transfer augmentation in a helical double-pipe heat exchanger, Heat Transfer 50 (2) (2021) 1872–1894, https://doi.org/10.1002/htj.21960.
[21] Mousavi Ajarostaghi, Seyed Soheil, et al., On the Hydrothermal behavior of fluid flow and heat transfer in a helical double-tube heat exchanger with curved swirl generator; impacts of length and position, Energies 16 (4) (2023) 1801, https://doi.org/10.3390/en16041801.
[22] K. Palanisamy, P.M. Kumar, Experimental investigation on convective heat transfer and pressure drop of cone helically coiled tube heat exchanger using carbon nanotubes/water nanofluids, Heliyon 5 (5) (2019) e01705, https://doi.org/10.1016/j.heliyon.2019.e01705.
[23] İbrahim Mahariq, Erciyas Atakan, A spectral element method for the solution of magnetostatic fields, Turk. J. Electr. Eng. Comput. Sci. 25 (4) (2017) 2922–2932, https://doi.org/10.3906/elk-1605-6.
[24] Ibrahim Mahariq, On the application of the spectral element method in electromagnetic problems involving domain decomposition, Turk. J. Electr. Eng. Comput. Sci. 25 (2) (2017) 1059–1069, https://doi.org/10.3906/elk-1511-115.
[25] Xiaogang Dong, et al., Deep learning with multilayer perceptron for optimizing the heat transfer of mixed convection equipped with MWCNT-water nanofluid, Case Stud. Therm. Eng. 57 (2024) 104309, https://doi.org/10.1016/j.csite.2024.104309.
[26] M.I.N. Ma'Arof, et al., Influence of fins designs, geometries and conditions on the performance of a plate-fin heat exchanger-experimental perspective, J. Mech. Eng. Sci. 13 (1) (2019) 4368–4379, https://doi.org/10.15282/jmes.13.1.2019.02.0372.
[27] Junlin Ye, et al., Performance analysis of spiral heat exchanger based on E-RPN and BWM multi-criteria decision algorithm-application of combined heat and power systems, Case Stud. Therm. Eng. 57 (2024) 104319, https://doi.org/10.1016/j.csite.2024.104319.